For submission to Earth and Planetary Science Letters

Multiple cosmogenic nuclides in glacial cobbles record Greenland exposure and erosion history

Lee B. Corbett*[a], Paul R. Bierman[a], Thomas A. Neumann[b], Joseph A. Graly[c], Jeremy D. Shakun[d]
Brent M. Goehring[e], Alan J. Hidy[f], and Marc W. Caffee[g,h]

*Corresponding Author: Ashley.Corbett@uvm.edu, (802) 380-2344
[a]Department of Geology, University of Vermont, Burlington, VT, USA
[b]Cryospheric Sciences Laboratory, NASA Goddard Space Flight Center, Greenbelt, MD, USA
[c]Department of Geography and Environmental Sciences, Northumbria University, Newcastle-upon-Tyne, UK
[d]Department of Earth and Environmental Sciences, Boston College, Boston, MA, USA
[e]Department of Earth and Environmental Sciences, Tulane University, New Orleans, LA, USA
[f]Center for Accelerator Mass Spectrometry, Lawrence Livermore National Laboratory, Livermore, CA, USA
[g]Department of Physics and Astronomy, Purdue University, West Lafayette, IN, USA
[h]Department of Earth, Atmospheric, and Planetary Sciences, Purdue University, West Lafayette, IN, USA

Abstract

The extent and erosivity of the Greenland Ice Sheet during the Pleistocene remain uncertain due to the paucity of evidence predating the Last Glacial Maximum. Here, we employ a novel approach, cosmogenic nuclide analysis of individual subglacial cobbles, which allows us to infer the behavior of the ice sheet over time and space. From three locations in western Greenland, we collected 86 cobbles from the current ice sheet margin and nine cobbles exposed on the modern proglacial land surface. We measured the concentration of in situ ^{10}Be in all cobbles (n = 95) and ^{26}Al and ^{14}C in a subset (n= 14). Cobbles deposited during Holocene retreat have ^{10}Be exposure ages generally consistent with the timing of ice retreat determined by other means. Conversely, most of the 86 subglacial cobbles contain very low concentrations of ^{10}Be (median 1.0 x 10^3 atoms g^{-1}), although several have ~10^4 and one has ~10^5 atoms g^{-1}. The low concentrations of ^{10}Be in most subglacial cobbles imply that their source areas under the Greenland Ice Sheet are deeply eroded, preserving minimal evidence of surface or near-surface exposure. The presence of measurable ^{14}C in ten of the cobbles requires that they experienced cosmogenic nuclide production within the past ~30 ka; however, ^{14}C/^{10}Be ratios of ~6 suggest that production occurred beneath thin overlying rock, sediment, and/or ice, where the muon component of ^{14}C production dominates. Only two of the 86 subglacial cobbles definitively have cosmogenic nuclide concentrations consistent with prior surface exposure during times of reduced ice extent. Overall, isotopic analysis of subglacial cobbles indicates that western Greenland's subglacial landscape is characterized by deep erosion and minimal subaerial exposure.

Keywords (n = 6): Cosmogenic nuclides; Greenland; Geochemistry; Isotopes; Pliocene; Pleistocene

1. Introduction

The Greenland Ice Sheet, its evolution over time, and its erosive capacity have been investigated extensively (as reviewed by Clark and Mix (2002), Funder et al. (2011), and Bierman et al. (2016)). However, despite previous work, ice sheet size remains poorly understood, especially over long (10^5-10^6 year) timescales (see Fig. 1 of Bierman et al. (2016)). Because each subsequent glaciation over-runs terrestrial deposits and landforms from previous glacial cycles (Gibbons et al., 1984), the study of subglacial erosion, landscape development, and ice sheet extent before the Last Glacial Maximum relies upon fragmentary and indirect evidence.

Here, we seek to assess long-term ice sheet extent and subglacial erosion using a novel approach: analysis of multiple cosmogenic nuclides in individual detrital cobbles sourced from beneath the Greenland Ice Sheet and transported to the ice margin by ice and/or subglacial water. We use 86 subglacial cobbles collected from the modern-day ice sheet margin and proximal outwash streams (Figs. 1 and 2), the cosmogenic nuclide concentrations of which record erosion and exposure over both time and space. The cobbles come from three regions in western Greenland with distinct landscapes and glaciological conditions. We also quantify ^{10}Be in nine additional surficial cobbles (three from each of the three sites) from the proglacial landscape to assess the effect of inherited cosmogenic nuclides on exposure dating.

Quantifying cosmogenic nuclide concentrations in detrital cobbles instead of at a single location (e.g., bedrock from the GISP2 ice core, Schaefer et al. (2016)) provides wider spatial coverage, allowing us to infer history and process across extensive subglacial sediment source areas. Although the source location and flow path of any individual cobble is unknowable and

45 the exposure and erosion history cannot be modeled uniquely, investigating a large number of
46 cobbles yields patterns and trends in cosmogenic nuclide concentrations. We assess common
47 themes in subglacial cobble cosmogenic nuclide concentrations and use those findings to make
48 inferences about western Greenland Ice Sheet history and erosional processes.
49
50 **2. Background**
51 *2.1. Using Multiple Cosmogenic Nuclides to Infer Cobble Exposure/Erosion History*
52 In situ produced cosmogenic nuclides, such as ^{10}Be, ^{26}Al, and ^{14}C, have been employed
53 for several decades to reconstruct glacial histories of exposed bedrock surfaces and moraine
54 boulders (Balco, 2011). These nuclides, produced predominately by neutron spallation
55 reactions (Lal and Peters, 1967) but also by muon interactions (Heisinger et al., 2002a;
56 Heisinger et al., 2002b) build up in rock at known rates over time. Because production by
57 neutron spallation decreases exponentially with depth with an e-folding length of about 70 cm,
58 subglacial erosion of several meters of rock strips most pre-existing spallation-produced
59 nuclides from a surface (Balco, 2011). Production by muon interactions (Heisinger et al., 2002a;
60 Heisinger et al., 2002b) occurs at lower rates and with a longer e-folding length, such that
61 muon-produced nuclides are present in rocks at low but measurable concentrations even after
62 glacial erosion has stripped several to tens of meters of surface material (Bierman et al., 2016;
63 Briner et al., 2016; Davis et al., 1999).
64 When multiple cosmogenic nuclides with different half-lives (e.g. ^{10}Be, 1.4 Ma; ^{26}Al, 0.7
65 Ma; and ^{14}C, 5.7 ka) are analyzed in the same sample, ratios of their concentrations provide
66 information about both exposure and burial (Briner et al., 2014). Nuclide production dominates

67 the inventories during the former, whereas loss through radioactive decay dominates the latter.
68 Pairing two longer-lived nuclides, such as $^{26}Al/^{10}Be$, provides information about exposure and
69 burial integrated over the past 10^5 to 10^6 years (Balco et al., 2014), but is relatively insensitive
70 to short durations of burial (less than several hundred kyr). Shorter-lived nuclides, such as ^{14}C,
71 are more sensitive to recent exposure, burial, and erosion (Briner et al., 2014; Miller et al.,
72 2006). Because the ^{14}C half-life is two orders of magnitude less than those of ^{10}Be and ^{26}Al,
73 measurable ^{14}C mandates spallation and/or muon production within ~30 ka.
74 Such multi-isotope approaches depend on knowing the ratio of the isotopes during
75 surface production, which serves as a benchmark for quantifying burial duration. For $^{26}Al/^{10}Be$,
76 the ratio of surface production is generally assumed to be ~6.75 (Balco et al., 2008), although
77 recent modeling (Argento et al., 2013) and empirical data (Corbett et al., 2017) suggest that the
78 value may be higher, at least in certain locations. For $^{14}C/^{10}Be$, the ratio of surface production,
79 albeit less well-constrained, is ~3-4 (Argento et al., 2013; Briner et al., 2014; Schimmelpfennig
80 et al., 2012). Ratios lower than production are indicative of burial following initial exposure, or
81 of prolonged surface exposure because the ratio decreases over time due to preferential decay
82 of the shorter-lived nuclide.
83 Because the production rates and ratios are dependent on depth, the ratios change as a
84 result of the relative proportion of the spallogenic and muogenic production (as reviewed in
85 Marrero et al. (2016)). Accounting for both production pathways, the $^{26}Al/^{10}Be$ production ratio
86 increases only slightly with depth, whereas the $^{14}C/^{10}Be$ and $^{14}C/^{26}Al$ production ratios increase
87 more appreciably with depth (Fig. 3). This occurs because the muogenic fraction of the total is
88 greater for ^{14}C than for ^{10}Be and ^{26}Al (~20% versus ~4% at the surface, respectively, and

increasing with depth, Lupker et al. (2015)). Therefore, although $^{14}C/^{10}Be$ and $^{14}C/^{26}Al$ are generally used to assess burial following initial exposure (Briner et al., 2014; Miller et al., 2006), nuclide ratios can also be used to assess shielding depth during exposure (Rand and Goehring, 2019).

2.2. Greenland Ice Sheet History/Process and Implications for Subglacial Cobble Nuclide Concentrations

2.2.1. Ice Sheet History and Possible Subglacial Cobble Exposure Periods

Although continental glaciation on Greenland may have occurred as early as the middle to late Miocene in East Greenland (Helland and Holmes, 1997; Larsen et al., 1994), expansive ice likely first occupied Greenland ~2.5 Ma, coincident with overall northern hemisphere cooling (Bierman et al., 2016; Flesche-Kleiven et al., 2002). Cobble source outcrops, which are all up-ice of the current interglacial ice margin, have been buried by ice for most of the Pleistocene.

In addition to being exposed to cosmic rays before the onset of glaciation (with varying degrees of partial shielding based on their depth of burial), the cobbles or their source outcrops could have been re-exposed when ice extent was reduced during warm periods of the Pleistocene (Schaefer et al., 2016). Interglacial sediments indicative of a warm Arctic exist in several locations around Greenland and are thought to be early Pleistocene in age (Funder et al., 2001). During MIS11 ~400 ka, pollen evidence (De Vernal and Hillaire-Marcel, 2008) and sediment provenance studies (Reyes et al., 2014) show that much of the southern Greenland Ice Sheet disappeared. The Eemian Period ~130 ka was characterized by appreciably reduced

ice extent as suggested by marine sediment provenance (Colville et al., 2011) and modeling (Helsen et al., 2013). Finally, the Greenland Ice Sheet was smaller than present for several thousand years during the warm middle Holocene as evidenced by lake sediment core records (Briner et al., 2010; Larsen et al., 2015).

Although nuclide production in the cobbles we analyzed could have occurred via neutron spallation during exposure in conjunction with these warm periods, muon production could also have occurred at depths of meters to tens of meters in the absence of surface exposure. Because muon production extends many meters through overlying material (Heisinger et al., 2002a; Heisinger et al., 2002b), nuclides could have been produced deep within cobble source outcrops before the onset of glaciation and/or in cobbles or source outcrops beneath overlying till, ice, or snow.

2.2.2. Glaciological Processes, Subglacial Erosion, and Cobble Plucking

In addition to recording ice sheet history, the cosmogenic nuclide concentrations of the cobbles we sampled are the result of ice sheet processes including subglacial erosion, plucking, freeze-on, and transport. The Greenland Ice Sheet began eroding parts of the underlying landscape as soon as glaciation began, and erosion continued throughout the Pliocene and Pleistocene, progressively eroding through the preglacial regolith and into bedrock at least in certain areas (Bierman et al., 2016). Cobbles were likely sourced from areas that at some point had basal temperatures at or near the pressure-melting point, in order for regelation to incorporate the cobbles into the ice matrix (Alley et al., 1997). However, basal conditions of the Greenland Ice Sheet are not well documented over space and time, and closely juxtapose

warm-based (erosive) and cold-based (non-erosive) ice (Petrunin et al., 2013). This spatial and temporal heterogeneity means that cobble source areas likely changed over time along with bed conditions.

The residence time of cobbles and sediment in the basal ice is largely determined by the relationships between the basal thermal state, the ice thickness, and the vertical and horizontal flow velocity. Cobbles are either incorporated into or shed from the ice depending on the thermal state at the ice-bed interface (Cuffey and Paterson, 2010). The along-flow advection rates of material within the ice varies from near zero at the ice sheet center to hundreds of meters per year near the margin (Cuffey and Paterson, 2010).

3. Study Sites

Our study focuses on three locations in western Greenland: Kangerlussuaq, Ilulissat, and Upernavik (Fig. 1). We chose these three sites because models suggest the ice sheet has responded to climate warmth differently at these locations, with more retreat near Kangerlussuaq, less retreat near Ilulissat, and little retreat near Upernavik (Helsen et al., 2013). The chronology of ice retreat and the likely timing of surficial cobble exposure is suggested by previous work at each of the three sites.

In Kangerlussuaq (67°N, -50°E), the landscape morphology and existing cosmogenic nuclide data are suggestive of deep glacial erosion. The region is characterized by a glacially-sculpted landscape of NE-SW elongated hills and lakes, carved parallel to the direction of ice flow. Rounded, striated bedrock is common. Till fills the valleys, whereas hilltops are typically bare rock. Numerous Holocene moraines are preserved; ^{10}Be analyses of moraine boulders

(Levy et al., 2012) cluster and match the local organic radiocarbon chronology, suggesting no or minimal inheritance of nuclides from previous exposure periods. Similarly, $^{26}Al/^{10}Be$ analyses of high-elevation bedrock surfaces in the area generally indicate deep erosion followed by a single period of exposure during the Holocene (Beel et al., 2016). Meteoric ^{10}Be concentrations in the fine-grained glacial sediment at Kangerlussuaq (n=17) are significantly lower than in other regions of Greenland, suggestive of effective subglacial erosion (Graly et al., 2018). Lake sediment core records show that the ice sheet near Kangerlussuaq was behind the current margin from ~7-4 ka (Larsen et al., 2015). The deposition of the three surficial cobbles we measured likely occurred ~6.8 ka based on the moraine chronology of Levy et al. (2012).

In Ilulissat (69°N, -50°E), the land surface and previously published cosmogenic nuclide data both suggest extensive glacial erosion, similar to in Kangerlussuaq. The landscape is glacially sculpted, heavily striated, and cut by numerous fjords. Most of the ice in the region drains through a large ice stream, Jakobshavn Isbræ. Holocene moraines are present and dozens of cosmogenic nuclide analyses (reviewed in Young et al. (2013)) suggest that ^{10}Be inheritance from previous exposure is minimal. Analysis of sediment cores from threshold lakes demonstrates that the ice margin retreated inland of its current position during the Holocene Climatic Optimum, reaching minimum extent from ~6-5 ka (Briner et al., 2010) or ~7-4 ka (Larsen et al., 2015) and remaining smaller than present until ~2 ka (Briner et al., 2010). The deposition of the three surficial cobbles we measured likely occurred ~7.8 ka based on the ages of a bedrock sample (GL080; 7.9 ± 0.2 ka) and a boulder sample (GL081; 7.6 ± 0.1 ka) collected from the same location as the cobbles (Corbett et al., 2011).

In Upernavik (~72°N, -54°E), unlike Kangerlussuaq and Ilulissat, the landscape morphology and existing cosmogenic nuclide data indicate that glacial erosion was heterogeneous and limited. The region has large relief, characterized by table-top highlands cut by deep fjords. Although some low-elevation bedrock surfaces exhibit glacial rounding, the highlands show evidence of prolonged subaerial weathering including exfoliation, tors, and weathering pits. Analysis of ^{10}Be and ^{26}Al in Upernavik (Corbett et al., 2013) and south of Upernavik (Beel et al., 2016) indicates that the ice was cold-based and non-erosive at times in the past. At high elevations, multi-isotope analysis shows that surfaces preserve total histories of ~10^5-10^6 years, and even some low-elevation surfaces contain nuclides inherited from periods of exposure prior to the Holocene (Beel et al., 2016; Corbett et al., 2013). Meteoric ^{10}Be concentrations of fine-grained sediment entrained in the ice margin are higher here than in Kangerlussuaq or Ilulissat (Graly et al., 2018). The deposition of the three surficial cobbles we measured may have occurred ~12.1 ka based on the mean of ages from a bedrock sample (GU001; 13.6 $\pm$ 0.3 ka) and a boulder sample (GU002; 10.6 $\pm$ 0.3 ka) collected from the same location, or ~11 ka based on our best deglaciation estimate for the region (Corbett et al., 2013), although all of these estimates may be inflated by the presence of inherited ^{10}Be in the bedrock and boulder samples.

4. Methods

4.1. Study Design and Sample Collection

We measured in situ cosmogenic nuclides (^{10}Be in all; ^{26}Al and ^{14}C in a subset) in 86 subglacial cobble-sized rocks from Kangerlussuaq (n=33), Ilulissat (n=20), and Upernavik (n=33)

198 (Fig. 1, Supplementary Data Table S1). Most of these cobbles ("icebound cobbles", n = 62) were
199 sourced from sediment-laden basal ice exposed at the ice sheet margin or supraglacial debris
200 bands not near nunataks (Figs. 2A, 2B, 2C), while a smaller portion ("outwash cobbles", n = 24)
201 were sourced from ice-proximal channels just outside of large outwash tunnels (Fig. 2D). We
202 recorded information about cobble size, lithology, and angularity, and measured the location of
203 collection with a hand-held GPS (Table S1). Cobble lithologies vary, although most are quartz-
204 rich crystalline rocks including granite and gneiss; a much smaller portion are quartzite, breccia,
205 and schist.
206 We also analyzed ^{10}Be in an additional three surficial cobbles from each site (n = 9 total,
207 detailed in Table S1, Figs. 2E and 2F) from the modern proglacial landscape to assess whether
208 inherited ^{10}Be is detectable in samples that have been exposed since deglaciation. At two sites,
209 Ilulissat and Upernavik, we collected the surficial cobbles directly adjacent to a bedrock-boulder
210 sample pair. We purposefully selected cobbles of similar sizes to those collected at the ice
211 margin so that two populations are comparable. At all three sites, the surficial cobbles came
212 from high-elevation surfaces in comparison to the surrounding landscape with little/no present-
213 day sediment or vegetation cover. At each site, the cobbles were collected within close
214 proximity of each other, usually a few meters.
215
216 *4.2. Sample Preparation and Analysis*
217 Additional methodological detail can be found in the Supplementary Data and in Tables
218 S1-S5. For ^{10}Be and ^{26}Al, Samples were prepared at University of Vermont using procedures
219 described in Corbett et al. (2016). ^{10}Be/^{9}Be ratios were measured by accelerator mass

spectrometry (AMS) at Lawrence Livermore National Laboratory and corrected for a $^{10}Be/^{9}Be$ background ratio of $(4.2 \pm 1.6)\cdot10^{-16}$ (n = 24, Table S3). We chose a threshold ^{10}Be concentration of $3\cdot10^{3}$ atoms g^{-1} (exceeded by 14 of the 86 subglacial cobbles), above which we also analyzed ^{26}Al and ^{14}C. $^{26}Al/^{27}Al$ ratios were measured by AMS at Purdue Rare Isotope Measurement (PRIME) Laboratory and corrected for a $^{26}Al/^{27}Al$ background ratio of $(7.6 \pm 7.0)\cdot10^{-16}$ (n = 14, Table S3). For ^{14}C, sample preparation and measurement by AMS were conducted at University of Cologne (Fulop et al. (2015), Table S4).

For the nine surficial cobbles, we calculated exposure ages (Table S5) with the CRONUS Earth online exposure age calculator (Balco et al., 2008). We used the northeastern North American production rate calibration dataset and Lal/Stone scaling (see Supplementary Data).

4.3. Theoretical Models

To explore the concentrations of ^{10}Be and ^{26}Al under a long-lived, erosive ice sheet, we modeled the evolution of their concentrations in a bedrock profile using various exposure and erosion scenarios. Additional detail can be found in the Supplementary Data and in Figures S1-S2.

5. Results

For the 73 subglacial cobbles with $^{10}Be/^{9}Be$ detectable above background values, ^{10}Be concentrations are $(2.0 \pm 1.0)\cdot10^{2}$ to $(1.12 \pm 0.02)\cdot10^{5}$ atoms g^{-1} (Table S1), ranging over three orders of magnitude. The ^{10}Be concentrations form a right-skewed distribution with a median of $1.0\cdot10^{3}$ atoms g^{-1} and a mean of $4.2\cdot10^{3}$ atoms g^{-1} (Fig. 4). The ^{10}Be concentrations do not

242 form statistically separable populations (Fig. 5) based on type (icebound vs. outwash; t-test, p =
243 0.29), location (Kangerlussuaq, Ilulissat, Upernavik; ANOVA, p = 0.67), shape (angular,
244 subangular, subrounded, rounded; ANOVA, p = 0.46), or lithology (gneiss, granite, other;
245 ANOVA, p = 0.81).

246 The 14 subglacial cobbles with the highest ^{10}Be concentrations (>3·10^3 atoms g^{-1}, the
247 threshold used to determine which samples we analyzed for ^{26}Al and ^{14}C) also do not cluster
248 with regards to cobble characteristics (Table S1). They have varying lithologies and varying
249 shapes, ranging from subrounded to angular, although none of the 14 were well-rounded. They
250 came from both the ice margin itself as well as outwash deposits, with no systematic bias
251 toward one or the other.

252 ^{26}Al concentrations are (2.3 ± 0.3)·10^4 to (7.7 ± 0.3)·10^5 atoms g^{-1}. Resulting ^{26}Al/^{10}Be
253 ratios are 5.0 ± 1.1 to 8.4 ± 1.2 (n = 13, Tables 1 and S2, Fig. 6). In reference to the empirically-
254 determined Greenland ^{26}Al/^{10}Be surface production ratio of 7.3 (Corbett et al., 2017), none of
255 the cobbles are above the production ratio by >1σ, 7 are indistinguishable, and 6 are below by
256 >1σ. Conversely, in reference to the commonly-assumed ^{26}Al/^{10}Be surface production ratio of
257 6.75, 5 cobbles are above by >1σ, 5 are indistinguishable, and 3 are below by >1σ.

258 Of the cobbles analyzed for ^{14}C, three were below detection limit; the remaining ten ^{14}C
259 concentrations are (5.1 ± 1.4)·10^4 to (1.5 ± 0.2)·10^5 atoms g^{-1} (n = 13, Tables 1 and S4). All but
260 two samples have significant ^{14}C in excess of the steady state ^{14}C/^{10}Be surface production ratio
261 (Fig. 7). When ^{14}C/^{10}Be and ^{14}C/^{26}Al are plotted as regressions, all but the same two of the
262 samples lie along a trendline forming a significant linear relationship (R^2 = 0.92 for both
263 regressions); the slope of the regression is 5.92 for ^{14}C/^{10}Be and 0.76 for ^{14}C/^{26}Al (Fig. 8), both

well above the surface production ratios. The two samples not on the regression (GK015 and GU010) have higher ^{10}Be and ^{26}Al concentrations but lower ^{14}C concentrations than the remainder of the dataset (Fig. 7).

For the nine surficial cobbles, ^{10}Be concentrations are $(3.9 \pm 0.1)\cdot10^4$ to $(6.9 \pm 0.1)\cdot10^4$ atoms g^{-1} (Table S5). The average ^{10}Be concentrations by site are $(4.4 \pm 0.6)\cdot10^4$ for Kangerlussuaq, $(5.4 \pm 0.5)\cdot10^4$ for Ilulissat, and $(5.6 \pm 1.2)\cdot10^4$ for Upernavik (1SD, n = 3 for each), representing relative standard deviations of 12.5, 8.5, and 20.9%, respectively. When considered as exposure ages assuming constant exposure and no erosion, these translate to 6.8 ± 0.8 ka (Kangerlussuaq), 8.1 ± 0.7 ka (Ilulissat), and 7.8 ± 1.6 ka (Upernavik; n = 3, average, 1SD for each, Table S5).

6. Discussion

6.1. Subglacial Cobbles Generally Record Deep Subglacial Erosion

Most of the subglacial cobbles we measured have cosmogenic nuclide concentrations indicating deep erosion under ice without subsequent surface exposure. Long-exposed, high-latitude landscapes, such as the Tertiary preglacial Greenland land surface, would have had ^{10}Be concentrations of ~10^5-10^6 atoms g^{-1}, depending on subaerial erosion rates (see Bierman et al. (2016), their Figs. 2a and 4). The cobbles we measured had much lower ^{10}Be concentrations (13 below detection limit and an additional 37 with <10^3 atoms g^{-1}, Fig. 4), suggesting they were sourced from deeply-eroded outcrops with little exposure to cosmic radiation. Some of cobbles with low concentrations of ^{10}Be may have never experienced exposure at the surface; their nuclide inventories could be due to muogenic production at depth (Heisinger et al., 2002a;

286 Heisinger et al., 2002b) during shielding by overlying rock, sediment, and/or ice. The general
287 lack of ^{10}Be in the samples demonstrates that an uneroded or minimally eroded, subglacially-
288 preserved, Tertiary landscape was not the source material for the cobbles we collected.
289 However, all glacial detrital sediment records, including the cobbles we studied, are
290 biased toward areas of the ice sheet that generate significant volumes of sediment. The cobbles
291 were most likely derived from areas of warm-based ice, or areas that had warm-based ice
292 during at least one time, in order for plucking or freeze-on to have occurred. This over-
293 representation of erosive areas is similar to biases in records developed from marine sediment
294 cores (Bierman et al., 2016; Christ et al., 2019; Flesche-Kleiven et al., 2002; Helland and Holmes,
295 1997; Larsen et al., 1994) and studies of sediment emanating from glacial drainages (Nelson et
296 al., 2014). The cobbles therefore resulted from processes operating in sediment source areas
297 beneath the ice sheet, presumably areas of warm-based and erosive ice, rather than the
298 subglacial landscape as a whole.
299 Our estimates of subglacial erosion suggest that at least tens to more likely hundreds of
300 meters of rock have been removed from the cobble source landscapes since the onset of
301 glaciation. Theoretical models (Supplementary Data, Figs. S1 and S2) demonstrate that
302 subglacial erosion rates of ~20-50 m Myr^{-1} are needed to drive ^{10}Be concentrations in exhumed
303 material down to 10^3 atoms g^{-1} assuming thick, continuous ice cover since 2.5 Ma (the resulting
304 ^{10}Be concentrations are also sensitive to the assumed preglacial erosion rate, which we varied
305 from 5-50 m Myr^{-1}, Fig. S1). These erosion rates are minimum estimates, however, because the
306 relatively high ^{26}Al/^{10}Be ratios in our samples (~5-8) and bedrock from the bottom of the GISP2
307 ice core (~4; Schaefer et al. (2016)) indicate that interior Greenland experienced exposure

during the Pleistocene, which would increase nuclide concentrations (Fig. S2). High $^{26}Al/^{10}Be$ ratios are also consistent with muon production through thin, continuous ice cover for the past 2.5 Myr, but even higher erosion rates (> 50 m Myr^{-1}) in this case would be required to reduce ^{10}Be concentrations to 10^3 atoms g^{-1} (Fig. S1).

Overall, these findings are consistent with deep subglacial erosion and nuclides produced by muons (whether through thin ice or overlying bedrock) during the Pleistocene. These finding agree well with the quantitative estimates of subglacial erosion of Strunk et al. (2017), who used paired $^{26}Al/^{10}Be$ data from Greenland's coastal landscapes and a Monte Carlo approach tuned to the oxygen isotope record to conclude that low-lying landscapes (i.e. probable source areas for the cobbles we collected) have eroded at >50 m Ma^{-1} during the duration of ice cover. Similarly, Goehring et al. (2010) inferred 2-30 m of erosion during the last glacial cycle based on ^{10}Be in East Greenland ice-contact delta sediments.

6.2. The Greenland Ice Sheet: An (Imperfect) Erosion Machine

Within the spectrum of previously-published cosmogenic measurements of glacial materials in Greenland, our subglacial cobbles (median $1.0 \cdot 10^3$ atoms g^{-1}, mean $4.2 \cdot 10^3$ atoms g^{-1}) have ^{10}Be concentrations similar to sand emerging from the present-day subglacial drainage system via outwash streams in southern Greenland (mean = $6.5 \pm 4.1 \cdot 10^3$ atoms g^{-1}, n = 19, 1SD, Nelson et al. (2014)) and inheritance calculated from eastern Greenland glacial delta depth profiles (error-weighted mean = $6.9 \pm 1.0 \times 10^3$ atoms g^{-1}, n = 5, 1SD, Goehring et al. (2010), their Fig. 8). The detrital sediment assessed by both Nelson et al. (2014) and Goehring et al. (2010) is more similar to the mean than the median of the cobble data we present, likely

because subglacial erosion and transport homogenizes sediment, combining material from more- and less-eroded areas, an effect that we mimic with a large number of cobbles.

The ^{10}Be concentrations of Greenland's subglacial sediments (this study, Nelson et al. (2014), and Goehring et al. (2010)) are lower today than they were in the past. Analyses of East Greenland marine cores (Bierman et al., 2016) suggest that sediments shed off Greenland had appreciably more ^{10}Be in the late Miocene and Pliocene (~10^5 atoms g^{-1} with decay correction) and somewhat more ^{10}Be throughout the late Pliocene and early Pleistocene (~10^4 atoms g^{-1} with decay correction), not reaching ~10^3 atoms g^{-1} until about the past 1-2 Ma. Glacial diamict recovered in a west Greenland marine core from ~1.8 Ma has ^{10}Be concentrations as low as our cobbles (mean= 4.6 ± 2.0 ·10^3 atoms g^{-1}, n = 5, 1SD, (Christ et al., 2019)). The general decrease in ^{10}Be concentration over time and the low concentrations of ^{10}Be in Pleistocene and modern subglacial materials portrays the Greenland Ice Sheet as an erosive system that has (at least in certain locations) progressively excavated down into deep, seldom-exposed bedrock or sediments that are now being transported to the margin.

Concentrations of meteoric ^{10}Be in glacial sediment are appreciably higher than concentrations of in situ ^{10}Be. Graly et al. (2018) quantified meteoric ^{10}Be in the silt-sized sediment isolated from dirty basal ice at the same three locations from which we collected cobbles. Concentrations of meteoric ^{10}Be averaged 7·10^6 atoms g^{-1} in Kangerlussuaq and 2·10^7 atoms g^{-1} in both Ilulissat and Upernavik (Graly et al., 2018). These values are three to four orders of magnitude greater than the concentrations of in situ ^{10}Be in the cobbles, and are consistent with the high delivery rate of meteoric ^{10}Be in comparison to the production rate of in situ ^{10}Be. Graly et al. (2018) hypothesize that the high concentrations of measured ^{10}Be

suggest that the material they analyzed originated from preserved subglacial soils. The pronounced contrast between icebound silt and cobbles requires heterogeneity in the subglacial erosive system, with different sediment sizes being sourced from different environments.

Although cosmogenic nuclide analyses in detrital sediments generally indicate deep glacial erosion, other cosmogenic nuclide analyses around Greenland demonstrate that the ice sheet erodes its bed in some areas and not in others. The key difference appears to be between studies that investigate detrital sediments (that are therefore biased to sediment source areas) versus those that investigate material that is still in situ. The bottom of the GISP2 ice core from central Greenland preserves bedrock with an order of magnitude more ^{10}Be (9.8-24.8 $\cdot 10^3$ atoms g^{-1}, Schaefer et al. (2016)) than the subglacial cobbles considered here, and also contains sediments that are likely long-lived soils with high meteoric ^{10}Be concentrations (Bierman et al., 2014). Around Greenland's margins there are isolated regions of non-eroded bedrock, particularly at high elevations where the ice was likely cold-based and non-erosive, as demonstrated in both west (Beel et al., 2016; Corbett et al., 2013) and east (Håkansson et al., 2009) Greenland. Less erosive areas of the ice sheet do exist, both around the margins and in the interior, but are not represented in the detrital record since those uneroded, high-cosmogenic-nuclide-concentration landscapes are still in place.

6.3. Nuclide Production During Shielding

The presence of measurable in situ cosmogenic ^{14}C in the cobbles unequivocally demonstrates recent (within several tens of ka) production of cosmogenic nuclides. Because

374 the half-life of ^{14}C is so short (5.7 ka), any ^{14}C from before ~30ka has largely decayed away;
375 thus, the ^{14}C we measured indicates nuclide production during the latest Pleistocene or
376 Holocene. Recent nuclide production is further evidenced by the significant linear relationship
377 between ^{14}C with ^{10}Be and ^{26}Al (Fig. 8), as recent exposure and the resulting co-production of
378 ^{14}C, ^{10}Be, and ^{26}Al is the only mechanism to produce a correlation between the short-lived and
379 the long-lived nuclides.

380 It is likely that some or all of this nuclide production occurred when the cobbles were
381 partially shielded. The slope of the $^{14}C/^{10}Be$ regression formed by most of the cobbles is 5.9 (R^2
382 = 0.92, n = 8, Fig. 8), appreciably higher than the commonly accepted surface $^{14}C/^{10}Be$
383 production ratio of ~3-4 (Argento et al., 2013; Briner et al., 2014; Schimmelpfennig et al., 2012).
384 The higher than expected $^{14}C/^{10}Be$ is explained best by muogenic production during shielding
385 (Rand and Goehring, 2019), likely under a minimum shielding mass of ~200-250 g cm^{-2} (Fig. 3;
386 equivalent to ~75-95 cm of granitic rock). This is a minimum estimate because the $^{14}C/^{10}Be$ ratio
387 evolves towards lower values over time (Fig. 7), so the $^{14}C/^{10}Be$ at production would have been
388 higher than at the time of sample collection. Even four cobbles with no measurable ^{10}Be
389 contain ^{14}C (Fig. 8, see also Supplementary Data for detail), supporting the idea that the cobbles
390 were initially sourced from a depth with minimal ^{10}Be, and then ultimately shielded to a lesser
391 degree to accommodate ^{14}C production. Because muon production is a larger component of the
392 total production in ^{14}C than in ^{10}Be, it allows for the production of ^{14}C in the near-absence of
393 ^{10}Be under shielding.

394 Our results do not provide direct information about the composition of the material
395 (e.g., rock, sediment, and/or ice) that shielded the samples during the past ~30 ka, but we infer

396 that ice is the most likely. The observation that most cobbles (all except GK015 and GU010) fall
397 so closely along a line (Fig. 8) indicates that the cosmogenic nuclides they contain were
398 produced at the same time and under similar shielding conditions. It is difficult to imagine that
399 they were all plucked from the same depth within the bedrock profile, or that they were all
400 buried beneath the same thickness of sediment during the Holocene Climatic Optimum. It is
401 perhaps more reasonable to infer that nuclide production during partial shielding occurred
402 during the cobbles' journeys along glacial flow lines that took them upward and outward
403 toward the glacial margin. In this sense, if the cobbles all began their journey toward the ice
404 margin with different ^{10}Be concentrations but were subjected to similar shielded production of
405 ^{14}C and ^{10}Be through ice during transport, their resulting concentrations would form an
406 isochron. But regardless of whether shielding occurred by rock, sediment, ice, or a combination
407 thereof, the high ^{14}C/^{10}Be ratios generally reflect a cobble life cycle that is dominated by
408 shielding and nuclide production by muons.
409
410 *6.4. Interglacial Ice Sheet Retreat and Exposure*
411 Based on multiple nuclide data, only two of the 86 cobbles we analyzed unambiguously
412 experienced surface or near-surface exposure prior to ~30 ka: GK015 (subangular gneiss from
413 Kangerlussuaq) and GU010 (subangular granodiorite from Upernavik), both of which we
414 collected directly from the ice sheet margin. Both cobbles' ^{14}C/^{10}Be ratios can be explained with
415 spallogenic production (Fig. 7) and their concentrations fall significantly below the ^{14}C/^{10}Be and
416 ^{14}C/^{26}Al regression lines (Fig. 8), demonstrating a relative excess of the longer-lived nuclides.

417 The cobbles must have experienced at least some recent exposure, likely at depth as discussed
418 above and causing them to contain measurable ^{14}C, but they were also exposed prior to ~30 ka.
419 To assess exposure before ~30 ka, we can correct for recent nuclide production at depth
420 by removing the ^{10}Be and ^{26}Al that would have been co-produced with the measured ^{14}C. We
421 made this correction by using the measured ^{14}C concentration and the slopes of the $^{14}C/^{10}Be$
422 and $^{14}C/^{26}Al$ regressions to infer the concentrations of ^{10}Be and ^{26}Al that were co-produced with
423 ^{14}C (potentially during transport along flow lines toward the ice sheet margin), and subtracting
424 in order to estimate ^{10}Be and ^{26}Al before ~30 ka. This correction yields $^{26}Al/^{10}Be$ ratios of 5.76 $\pm$
425 0.36 for GK015 and 6.80 $\pm$ 0.26 for GU010.
426 After correcting the ^{10}Be and ^{26}Al concentrations for recent production, the pre-~30ka
427 exposure/burial histories of these two cobbles likely differ in both duration and timing. For
428 sample GK015, the corrected $^{26}Al/^{10}Be$ ratio (5.76 $\pm$ 0.36) is below the $^{26}Al/^{10}Be$ production ratio
429 (regardless of whether we assume a surface production ratio of 7.3 or 6.75) beyond 1σ
430 uncertainties, which could be explained by either burial following exposure or prolonged
431 exposure that caused the $^{26}Al/^{10}Be$ ratio to drop due to the shorter half-life of ^{26}Al (Balco et al.,
432 2014). In the case of the former, initial exposure could not have occurred exclusively during
433 MIS5e because the duration of intervening burial would be insufficient to cause a detectable
434 departure from the production ratio, although it could have been re-exposed during MIS5e in a
435 multi-stage exposure scenario. Sample GU010 has a higher corrected $^{26}Al/^{10}Be$ ratio (6.80 $\pm$
436 0.26), likely indicating surface exposure during a more recent warm period (and perhaps during
437 older periods as well). Its ^{10}Be concentration is the highest of the 86 cobbles we measured,

requiring at least ~25 ka of surface exposure at sea level (less at higher elevations); accordingly, this inventory of ^{10}Be could not have built up only during the Holocene Climatic Optimum. Its cosmogenic nuclide inventory is a product of multiple periods of exposure, likely including MIS5e and perhaps previous interglacials as well.

6.5. Cosmogenic Nuclide Inheritance and Implications for Dating Studies

Measurable, if low, in situ cosmogenic nuclides in most subglacial cobbles implies that even extensive, long-lived glacial erosion is unable to fully "reset" the cosmogenic clock (Briner et al., 2016; Davis et al., 1999; Rand and Goehring, 2019). Our dataset provides two complementary lines of evidence for the presence of muon-produced nuclides: (1) low but pervasive ^{10}Be concentrations (median 10^3 atoms g^{-1}) and (2) ^{14}C/^{10}Be and ^{14}C/^{26}Al co-production at ratios definitively higher than those of surface production. Small concentrations of primarily muon-produced nuclides are likely present in many glacial environments, not only in moraine boulders and glacially-sculpted bedrock as is frequently analyzed (Balco, 2011), but also in detrital sediment (Goehring et al., 2010; Nelson et al., 2014).

Although inherited ^{10}Be is probably present in most cobbles transported to the ice sheet margin, its impact on inferred exposure ages depends on the relative portion of inherited ^{10}Be versus ^{10}Be produced during the current period of exposure (Fig. 9). The median subglacial cobble ^{10}Be concentration is ~10^3 atoms g^{-1}, equivalent to about 250 years of surface exposure at high latitude; this represents a relatively small effect on the age of a latest Pleistocene moraine, but a very appreciable effect on the age of a Little Ice Age moraine. However, a subset of the subglacial cobbles we analyzed contained higher ^{10}Be concentrations, which would

460 appreciably skew exposure ages for any dating application; for example, GU010 contains ~10^5
461 atoms g^{-1} of ^{10}Be, the equivalent of ~25 ky of surface exposure at sea level and high latitude.
462 The nine surficial cobbles we collected and analyzed exhibit scatter in their ^{10}Be
463 concentrations and inferred ages (Fig. 9, Table S5). ^{10}Be concentrations of these cobbles (n = 3
464 per site) are not consistent within 1σ analytic uncertainties (Fig. 9), despite being collected
465 within close proximity. Such variance could reflect shielding (e.g., by snow, ice, or till since
466 deposition, which may be more important for small cobbles than for large boulders) and/or the
467 presence of inherited produced ^{10}Be.
468 Cobble exposure ages (Fig. 9, Table S5) agree with independent estimates of
469 deglaciation timing better in certain locations than in others. In Kangerlussuaq, the mean
470 surficial cobble age (6.8 ± 0.8 ka; Fig. 9) is consistent with the age of deglaciation inferred from
471 the moraine chronology of Levy et al. (2012). In Ilulissat, the mean surficial cobble age (8.1 $\pm$ 0.7
472 ka; Figs. 2E and 9) is indistinguishable from a bedrock sample (GL080; 7.9 $\pm$ 0.2 ka) and a
473 boulder sample (GL081; 7.6 $\pm$ 0.1 ka) collected from the same location (Corbett et al., 2011).
474 These observations are consistent with the findings of Briner et al. (2013), who reported cobble
475 exposure ages similar to boulder and bedrock ages in central western Greenland, a landscape
476 deeply scoured by erosive warm-based ice. However, in Upernavik, the mean surficial cobble
477 age (7.8 $\pm$ 1.6 ka; Figs. 2F and 9) is younger than a bedrock sample (GU001; 13.6 $\pm$ 0.3 ka) and a
478 boulder sample (GU002; 10.6 $\pm$ 0.3 ka) collected from the same location (Corbett et al., 2013).
479 This offset likely reflects the effect of snow or till cover on the small cobble samples and/or ^{10}Be
480 inheritance in the bedrock and boulder samples. The Upernavik area shows strong evidence for

non-erosive, cold-based ice (Beel et al., 2016; Corbett et al., 2013), which may lead to disagreement between exposure ages inferred from bedrock, boulders, and cobbles.

7. Conclusions

Analysis of cosmogenic nuclides in 86 subglacial cobbles and 9 surficial cobbles from western Greenland demonstrates that detrital material currently emerging at the ice sheet margin has cosmogenic nuclide concentrations generally indicative of deep erosion. Most subglacial cobbles contain little ^{10}Be, only ~10^3 atoms g^{-1}, suggesting they were sourced from depth and have experienced little exposure since they were quarried. Although less erosive areas of the ice sheet exist and are documented in other studies, they are not well-represented in detrital sediment samples, which originate from areas of warm-based, erosive ice. Measurable ^{14}C in some subglacial cobbles indicates recent nuclide production, within the past ~30 ka; however, ^{14}C/^{10}Be ratios above that of surface production indicate that nuclide production occurred under shielding. Only two subglacial cobbles have ^{14}C/^{10}Be and ^{14}C/^{26}Al ratios indicative of excess longer-lived nuclides; their ^{10}Be and ^{26}Al concentrations can be explained by surface or near-surface exposure predating the timespan recorded by ^{14}C. Surficial cobbles exhibit scatter in their ^{10}Be concentrations beyond analytic uncertainties, and match deglaciation age estimates better in certain areas than in others. Overall, the nuclide concentrations of 95 glacial cobbles demonstrate that muon-produced nuclides are pervasive even in long-buried and deeply-eroded landscapes. Although inherited ^{10}Be is generally present in small concentrations, it is occasionally present in concentrations high enough to influence exposures ages.

Acknowledgements
Support for this research was provided by NSF ARC-0713956, NSF ARC-1023191, a NSF Doctoral Dissertation Research Improvement Grant (BCS-1433878), and an NSF Graduate Research Fellowship. Corbett's time was partially supported by NSF EAR-1735676. Field support was provided by CH2MHILL. We thank R. Finkel for assistance with ^{10}Be measurements at Lawrence Livermore National Laboratory, performed under the auspices of the U.S. Department of Energy under contract DE-AC52-07NA27344. Work at PRIME Laboratory was supported by NSF EAR-0919759. We thank T. Dunai for conducting ^{14}C measurements at University of Cologne.

References

Alley, R., Cuffey, K., Evenson, E., Strasser, J., Lawson, D., Larson, G., 1997. How glaciers entrain and transport basal sediment: physical constraints. Quaternary Science Reviews 16, 1017-1038.

Argento, D., Reedy, R., Stone, J., 2013. Modeling the earth's cosmic radiation. Nuclear Instruments and Methods in Physics Research B 294, 464-469.

Balco, G., 2011. Contributions and unrealized potential contributions of cosmogenic-nuclide exposure dating to glacier chronology, 1990-2010. Quaternary Science Reviews 30, 3-27.

Balco, G., 2017. Production rate calculations for cosmic-ray-muon-produced ^{10}Be and ^{26}Al benchmarked against geological calibration data. Quaternary Geochronology 39, 150-173.

Balco, G., Stone, J., Sliwinsku, M., Todd, C., 2014. Features of the glacial history of the Transantarctic Mountains inferred from cosmogenic ^{26}Al, ^{10}Be and ^{21}Ne concentrations in bedrock surfaces. Antarctic Science 26, 708-723.

Balco, G., Stone, J.O., Lifton, N.A., Dunai, T.J., 2008. A complete and easily accessible means of calculating surface exposure ages or erosion rates from ^{10}Be and ^{26}Al measurements. Quaternary Geochronology 3, 174-195.

Beel, C., Lifton, N., Briner, J., Goehring, B., 2016. Quaternary evolution and ice sheet history of contrasting landscapes in Uummannaq and Sukkertoppen, western Greenland. Quaternary Science Reviews 149, 248-258.

Bierman, P., Corbett, L., Graly, J., Neumann, T., Lini, A., Crosby, B., Rood, D., 2014. Preservation of a preglacial landscape under the center of the Greenland Ice Sheet. Science 344, 402-405.

Bierman, P., Shakun, J., Corbett, L., Zimmerman, S., Rood, D., 2016. A persistent and dynamic East Greenland Ice Sheet over the past 7.5 million years. Nature 540, 256-260.

Briner, J., Hakansson, L., Bennike, O., 2013. The deglaciation and neoglaciation of Upernavik Isstrøm, Greenland. Quaternary Research 80, 459-467.

Briner, J., Stewart, H., Young, N., Phillips, W., Losee, S., 2010. Using proglacial-threshold lakes to constrain fluctuations of the Jakobshavn Isbrae ice margin, western Greenland, during the Holocene. Quaternary Science Reviews 29, 3861-3874.

Briner, J.P., Goehring, B.M., Mangerud, J., Svendsen, J.I., 2016. The deep accumulation of ^{10}Be at Utsira, southwestern Norway: Implications for cosmogenic nuclide exposure dating in peripheral ice sheet landscapes. Geophysical Research Letters 43, 9121-9129.

Briner, J.P., Lifton, N.A., Miller, G.H., Refsnider, K., Anderson, R., Finkel, R., 2014. Using in situ cosmogenic ^{10}Be, ^{14}C, and ^{26}Al to decipher the history of polythermal ice sheets on Baffin Island, Arctic Canada. Quaternary Geochronology 19, 4-13.

Christ, A., Bierman, P., Knutz, P., Corbett, L.B., Fosdick, J., Thomas, E., Cowling, O., Hidy, A., Caffee, M., 2019. The northwestern Greenland Ice Sheet during the early Pleistocene was similar to today. Geophysical Research Letters 47, GL085176.

Clark, P., Mix, A., 2002. Ice sheets and sea level of the Last Glacial Maximum. Quaternary Science Reviews 21, 1-7.

Colville, E., Carlson, A., Beard, B., Hatfield, R., Stoner, J., Reyes, A., Ullman, D., 2011. Sr-Nd-Pb isotope evidence for ice-sheet presence on southern Greenland During the Last Interglacial. Science 333, 620-623.

Corbett, L., Bierman, P., Rood, D., Caffee, M., Lifton, N., Woodruff, T., 2017. Cosmogenic $^{26}Al/^{10}Be$ Surface Production Ratio in Greenland. Geophysical Research Letters 44, 1350-1359.

Corbett, L., Young, N., Bierman, P., Briner, J., Neumann, T., Graly, J., Rood, D., 2011. Paired bedrock and boulder ^{10}Be concentrations resulting from early Holocene ice retreat near Jakobshavn Isfjord, western Greenland. Quaternary Science Reviews 30, 1739-1749.

Corbett, L.B., Bierman, P.R., Graly, J.A., Neumann, T.A., Rood, D.H., 2013. Constraining landscape history and glacial erosivity using paired cosmogenic nuclides in Upernavik, northwest Greenland. Geological Society of America Bulletin 125, 1539-1553.

Corbett, L.B., Bierman, P.R., Rood, D.H., 2016. An approach for optimizing in situ cosmogenic ^{10}Be sample preparation. Quaternary Geochronology 33, 24-34.

Cuffey, K., Paterson, W., 2010. The Physics of Glaciers, Fourth Edition ed. Academic Press.

Davis, P., Bierman, P., Marsella, K., Caffee, M., Southon, J., 1999. Cosmogenic analysis of glacial terrains in the eastern Canadian Arctic: a test for inherited nuclides and the effectiveness of glacial erosion. Annals of Glaciology 28.

De Vernal, A., Hillaire-Marcel, C., 2008. Natural variability of Greenland climate, vegetation, and ice volume during the past million years. Science 320, 1622-1625.

Flesche-Kleiven, H., Jansen, E., Fronval, T., Smith, T., 2002. Intensification of Northern Hemisphere glaciations in the circum Atlantic region (3.5–2.4 Ma) – ice-rafted detritus evidence. Palaeogeography, Palaeoclimatology, Palaeoecology 184, 213-223.

Fulop, R., Wacker, L., Dunai, T., 2015. Progress report on a novel in situ ^{14}C extraction scheme at the University of Cologne. Nuclear Instruments and Methods Section B: Beam Interactions with Materials and Atoms 361, 20-24.

Funder, S., Bennike, O., Bocher, J., Israelson, C., Petersen, K., Simonarson, L., 2001. Late Pliocene Greenland- The Kap Kobenhavn Formation in North Greenland. Bulletin of the Geological Society of Denmark 48, 117-134.

Funder, S., Kjeldsen, K., Kjær, K., Cofaigh, C., 2011. The Greenland Ice Sheet during the past 300,000 years: A review. Developments in Quaternary Science 15, 699-713.

Gibbons, A., Megeath, J., Pierce, K., 1984. Probability of moraine survival in a succession of glacial advances. Geology 12, 327-330.

Goehring, B., Kelly, M., Schaefer, J., Finkel, R., Lowell, T., 2010. Dating of raised marine and lacustrine deposits in east Greenland using beryllium-10 depth profiles and implications for estimates of subglacial erosion. Journal of Quaternary Science 25, 865-874.

Graly, J., Corbett, L., Bierman, P., Lini, A., Neumann, T., 2018. Meteoric ^{10}Be as a tracer of subglacial processes and interglacial surface exposure in Greenland. Quaternary Science Reviews 191, 118-131.

Håkansson, L., Alexanderson, H., Hjort, C., Moller, P., Briner, J., Aldahan, A., Possnert, G., 2009. Late Pleistocene glacial history of Jameson Land, central East Greenland, derived from cosmogenic ^{10}Be and ^{26}Al exposure dating. Boreas 38, 244-260.

Heisinger, B., Lal, D., Jull, A., Kubik, P., Ivy-Ochs, S., Knie, K., Nolte, E., 2002a. Production of selected cosmogenic radionuclides by muons: 2. Capture of negative muons. Earth and Planetary Science Letters 200, 357-369.

Heisinger, B., Lal, D., Jull, A., Kubik, P., Ivy-Ochs, S., Neumaier, S., Knie, K., Lazarev, V., Nolte, E., 2002b. Production of selected cosmogenic radionuclides by muons: 1. Fast muons. Earth and Planetary Science Letters 200, 345-355.

Helland, P., Holmes, M., 1997. Surface Textural Analysis of Quartz Sand Grains from ODP Site 918 Off the Southeast Coast of Greenland Suggests Glaciation of Southern Greenland at 11 Ma. Palaeogeography, Palaeoclimatology, Palaeoecology 135, 109-121.

Helsen, M., Van De Berg, W., Van De Wal, R., Van Den Broeke, M., Oerlemans, J., 2013. Coupled regional climate–ice sheet simulation shows limited Greenland ice loss during the Eemian. Climate of the Past 9.

Lal, D., Peters, B., 1967. Cosmic Ray Produced Radioactivity on the Earth, Encyclopedia of Physics. Springer, Berlin, pp. 551-612.

Larsen, H., Saunders, A., Clift, P., Beget, J., Wei, W., Spezzaferri, S., 1994. Seven million years of glaciation in Greenland. Science 264, 952-955.

Larsen, N., Hjaer, K., Lecavalier, B., Bjork, A., Colding, S., Huybrechts, P., Jakobsen, K., Kjeldsen, K., Knudsen, K., Odgaard, B., Olsen, J., 2015. The response of the southern Greenland ice sheet to the Holocene thermal maximum. Geology 43, 291-294.

Levy, L., Kelly, M., Howley, J., Virginia, R., 2012. Age of the Ørkendalen moraines, Kangerlussuaq, Greenland: constraints on the extent of the southwestern margin of the Greenland Ice Sheet during the Holocene. Quaternary Science Reviews 52, 1-5.

Lupker, M., Hippe, K., Wacker, L., Kober, F., Maden, C., Braucher, R., Bourles, D., Vidal Romani, J., Wieler, R., 2015. Depth-dependence of the production rate of in situ ^{14}C in quartz from the Leymon High core, Spain. Quaternary Geochronology 28, 80-87.

Marrero, S., Phillips, F., Borchers, B., Lifton, N., Aumer, R., Balco, G., 2016. Cosmogenic nuclide systematics and the CRONUScalc program. Quaternary Geochronology 31, 160-187.

Miller, G.H., Briner, J.P., Lifton, N.A., Finkel, R.C., 2006. Limited ice-sheet erosion and complex exposure histories derived from in situ cosmogenic ^{10}Be, ^{26}Al, and ^{14}C on Baffin Island, Arctic Canada. Quaternary Geochronology 1, 74-85.

Nelson, A., Bierman, P., Shakun, J., Rood, D., 2014. Using in situ cosmogenic ^{10}Be to identify the source of sediment leaving Greenland. Earth Surface Processes and Landforms 39, 1087-1100.

Petrunin, A., Rogozhina, I., Vaughan, A., Kukkonen, I., Kaban, M., Koulakov, I., Thomas, M., 2013. Heat flux variations beneath central Greenland/'s ice due to anomalously thin lithosphere. Nature Geoscience 6, 746-750.

Rand, C., Goehring, B., 2019. The distribution and magnitude of subglacial erosion on millennial timescales at Engabreen, Norway. Annals of Glaciology 60, 73-81.

Reyes, A., Carlson, A., Beard, B., Hatfield, R., Stoner, J., Winsor, K., Welke, B., Ullman, D., 2014. South Greenland ice-sheet collapse during Marine Isotope Stage 11. Nature 510, 525-528.

Schaefer, J., Finkel, R., Balco, G., Alley, R., Caffee, M., Briner, J., Young, N., Gow, A., Schwartz, R., 2016. Greenland was nearly ice-free for extended periods during the Pleistocene. Nature 540, 252-255.

Schimmelpfennig, I., Schaefer, J., Goehring, B., Lifton, N., Putnam, A., Barrell, D., 2012. Calibration of the in situ cosmogenic ^{14}C production rate in New Zealand's Southern Alps. Journal of Quaternary Science 27, 671-674.

Strunk, A., Knudsen, M., Egholm, D., Jansen, J., Levy, L., Jacobsen, B., Larsen, N., 2017. One million years of glaciation and denudation history in west Greenland. Nature Communications 8.

Young, N., Briner, J., Rood, D., Finkel, R., Corbett, L., Bierman, P., 2013. Age of the Fjord Stade moraines in the Disko Bugt region, western Greenland, and the 9.3 and 8.2 ka cooling events. Quaternary Science Reviews 60, 76-90.

Table and Figure Captions

Table 1. Isotopic concentrations and uncertainties for the cobbles with ^{10}Be, ^{26}Al, and ^{14}C data. All 95 ^{10}Be measurements are shown in Table S1. Analysis details including measured ratios, background-corrected ratios, AMS cathode numbers, and primary standards are shown in Tables S1 (for ^{10}Be), S2 (for ^{26}Al), and S4 (for ^{14}C). Blanks for ^{10}Be and ^{26}Al are detailed in Table S3.

Figure 1. Map of Greenland showing the three locations from which cobble-sized rocks were collected from the present-day ice sheet margin. "Icebound" cobbles were embedded directly in the ice, whereas "outwash" cobbles are from large outwash tunnels proximal to the ice sheet margin; both are "subglacial". Conversely, "surficial" cobbles are from the proglacial landscape and have presumably been exposed since deglaciation. Also shown are other cosmogenic isotope records of subglacial sediments as discussed in the text.

Figure 2. Photographs of environments from which subglacial cobbles were collected. Panel A: Ice margin near Upernavik showing sediment-rich basal ice containing icebound cobbles. Panel B: Chipping an icebound cobble out of the margin near Kangerlussuaq. Panel C: Representative icebound cobble from dirty basal ice exposed at the margin near Kangerlussuaq. Panel D: View of an outwash tunnel near Kangerlussuaq where outwash cobbles were sampled from channel bars proximal to the ice margin (note people in the foreground for scale). Panel E: The location in Ilulissat at which we sampled surficial cobbles as well as the bedrock surface and a boulder (Corbett et al., 2011). Panel F: The location in Upernavik at which we sampled surficial cobbles as well as the bedrock surface and a boulder (Corbett et al., 2013).

Figure 3. Theoretical models of ^{10}Be production (dark gray lines) and ^{14}C production (light gray lines) by both spallation (thick lines) and muons (thin lines) as a function of depth. Shown also is the resulting ^{14}C/^{10}Be ratio (heavy black line). Depth is expressed in terms of mass depth. All curves assume sea level production in central western Greenland. ^{14}C spallation production rates are derived from measurements of CRONUS-A material extracted in the Tulane cosmogenic nuclide lab (B.M. Goehring, unpublished data, n = 20), and ^{14}C muon production rates are from (Balco, 2017).

Figure 4. Probability density function of ^{10}Be concentrations of subglacial cobbles (n = 73 above detection limit). Thin gray lines represent the measured isotopic concentrations and internal uncertainties for each sample; thick black line represents the summed probability. Sample names are shown for the cobbles with the highest ^{10}Be concentrations (see Table 1 for detail). Inset: Histogram of ^{10}Be concentrations of the 86 subglacial cobbles we analyzed for ^{10}Be (including 13 that were below detection limit); note logarithmic scale on the x-axis.

Figure 5. Box plots based on four different metrics (location, type, angularity, and lithology) for describing the ^{10}Be concentrations of the subglacial cobbles. Each population includes 73 total subglacial cobbles that were above detection limit for ^{10}Be. The heavy black line shows the mean, while the dashed black line shows the median; the top and bottom of the box show the mean $\pm$ 1SD.

Figure 6. ^{26}Al-^{10}Be paired nuclide plot for 13 subglacial cobbles. The thick and thin black curves show the continuous exposure pathway and steady-states with respect to steady erosion endpoints respectively for the Greenland ^{26}Al/^{10}Be production ratio of 7.3 (based on Corbett et al. (2017)). The thick and thin gray curves show the constant production pathway and erosion endpoints for the commonly-assumed ^{26}Al/^{10}Be production ratio of 6.75.

Figure 7. Paired ^{14}C/^{10}Be plot for 10 subglacial cobbles with detectable ^{14}C presented in terms of production rate normalized ^{14}C/^{10}Be ratio and ^{10}Be concentrations. Normalization was made assuming the ^{14}C and ^{10}Be production rates for sea level and high latitude. Error ellipses are shown at the 68% confidence level. All but two of the samples plot above the field of continuous exposure, one sample is consistent with continuous exposure, and another sample is consistent with at least one period of exposure and burial.

Figure 8. Linear regressions of ^{14}C concentration versus ^{10}Be concentration (top panel, n = 10) and ^{26}Al concentration (bottom panel, n = 9) for subglacial cobbles. Regressions are for samples symbolized with gray dots; those with white dots (samples with ^{10}Be below detection limit) and black dots (samples enriched in the long-lived isotopes) are not included in the regression.

Figure 9. ^{10}Be concentrations (top panel) and inferred exposure ages (bottom panel) of surficial cobbles from well outside the modern-day ice margin (n = 3 per site, detail in Table S5). Cobbles at each site were collected from the same location, all within several meters of one another. Error bars show 1σ analytic uncertainties (not visible in all cases). Gray lines show the average concentration/age at each site, and the gray box shows $\pm$ 1SD. Dashed lines denote comparisons. Photographs of the sites at which cobbles, the bedrock surface, and a boulder were all sampled are shown in Fig. 2E (Ilulissat) and 2F (Upernavik).

Sample Name	^{10}Be Concentration (atoms g^{-1})[a]	1σ ^{10}Be Uncertainty (atoms g^{-1})[a]	^{26}Al Concentration (atoms g^{-1})[b]	1σ ^{26}Al Uncertainty (atoms g^{-1})[b]	^{26}Al/^{10}Be Ratio	1σ ^{26}Al/^{10}Be Uncertainty	^{14}C Concentration (atoms g^{-1})[c]	1σ ^{14}C Uncertainty (atoms g^{-1})[c]	^{14}C/^{10}Be Ratio	1σ ^{14}C/^{10}Be Uncertainty
GK015	3.26E+04	5.67E+02	2.16E+05	1.30E+04	6.64	0.42	8.32E+04	8.60E+03	2.56	0.27
GK022	1.10E+04	3.09E+02	7.28E+04	4.44E+03	6.64	0.45	1.24E+05	9.50E+03	11.31	0.92
GK040	4.85E+03	4.25E+02	2.41E+04	4.95E+03	4.98	1.11	6.48E+04	1.74E+04	13.37	3.78
GK051	8.32E+03	2.76E+02	ND	ND	ND	ND	9.09E+04	2.52E+04	10.92	3.05
GK070	4.29E+03	3.04E+02	3.44E+04	3.06E+03	8.03	0.91	BDL	BDL	ND	ND
GK071	4.06E+03	2.25E+02	3.08E+04	4.31E+03	7.59	1.14	7.90E+04	8.70E+03	19.45	2.40
GK072	3.53E+03	1.68E+02	2.34E+04	2.96E+03	6.61	0.89	BDL	BDL	ND	ND
GK097	1.82E+04	4.12E+02	1.37E+05	1.18E+04	7.52	0.67	ND	ND	ND	ND
GK099	1.18E+04	3.09E+02	8.67E+04	6.85E+03	7.37	0.61	BDL	BDL	ND	ND
GL028	5.00E+03	2.08E+02	2.97E+04	2.61E+03	5.93	0.58	6.91E+04	9.10E+03	13.81	1.91
GL036	3.99E+03	2.15E+02	3.34E+04	4.40E+03	8.38	1.19	6.60E+04	8.50E+03	16.55	2.31
GU010	1.12E+05	2.23E+03	7.71E+05	2.51E+04	6.87	0.26	5.10E+04	1.37E+04	0.45	0.12
GU034	7.38E+03	3.94E+02	3.92E+04	3.21E+03	5.31	0.52	7.81E+04	9.00E+03	10.58	1.34
GU126	1.89E+04	4.18E+02	1.42E+05	1.18E+04	7.52	0.65	1.51E+05	1.50E+04	8.00	0.81

[a]The ^{10}Be/^{9}Be measurements were made at Lawrence Livermore National Laboratory and were normalized to standard 07KNSTD3110 with an assumed ratio of 2.85 x 10^{-11} (Nishiizumi et al., 2007).

[b]The ^{26}Al/^{27}Al measurements were made at Purdue Rare Isotope Measurement Laboratory and were normalized to standard KNSTD with an assumed ratio of 1.818 x 10^{-12} (Nishiizumi et al., 2004).

[d]The ^{14}C measurements were made at University of Cologne.

ND = No data (sample failed during measurement yielding no usable data)

BDL = Below detection limit (see text for details)

Table 1.

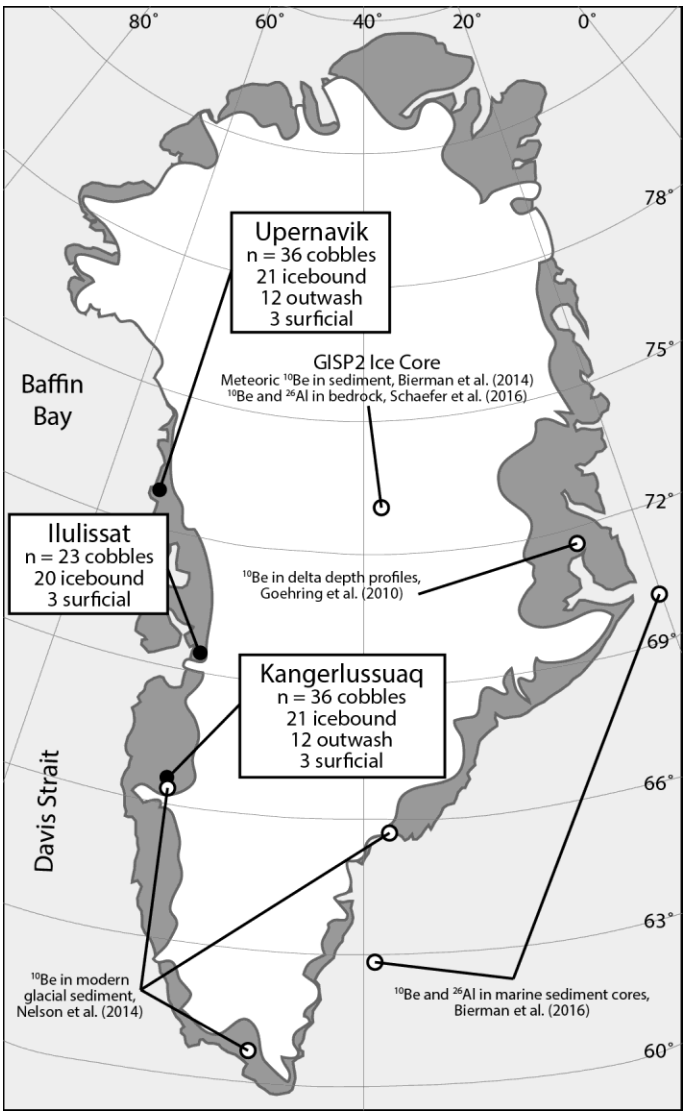

Figure 1.
(Width = 90mm, one column)

Figure 2.
(width = 190 mm, full page with caption below)

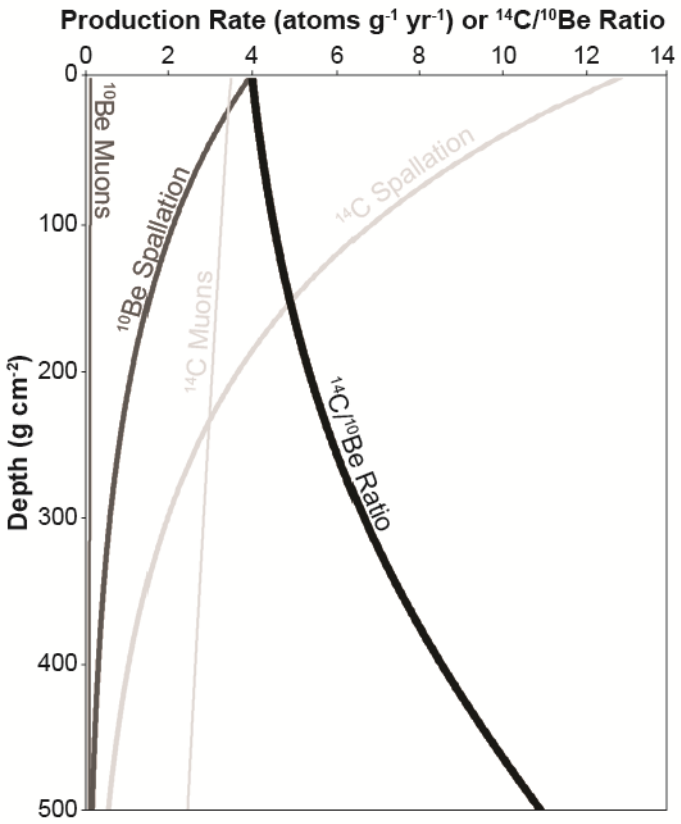

Figure 3.
(Width = 90 mm, one column)

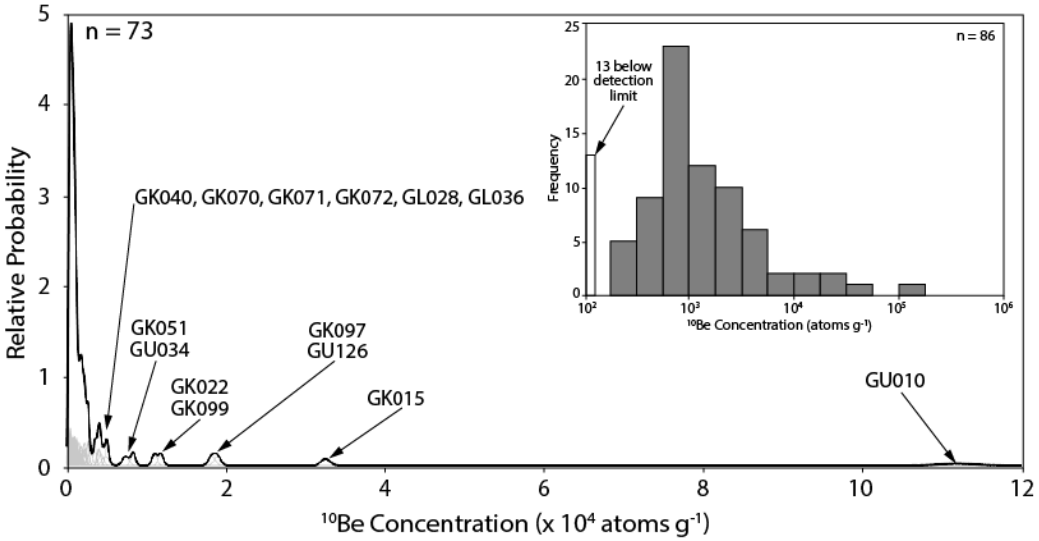

Figure 4.
(Width = 140 mm, 1.5 columns)

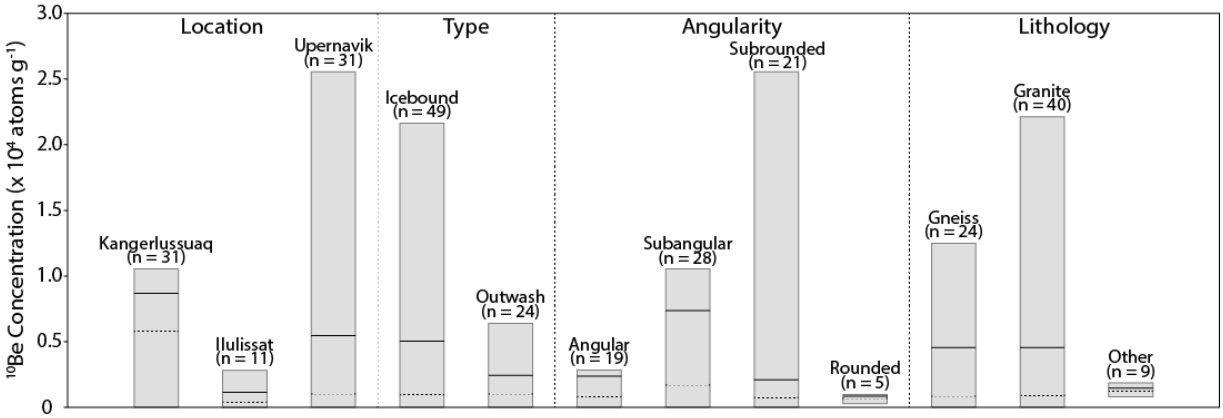

Figure 5.
(Width = 190 mm, full page)

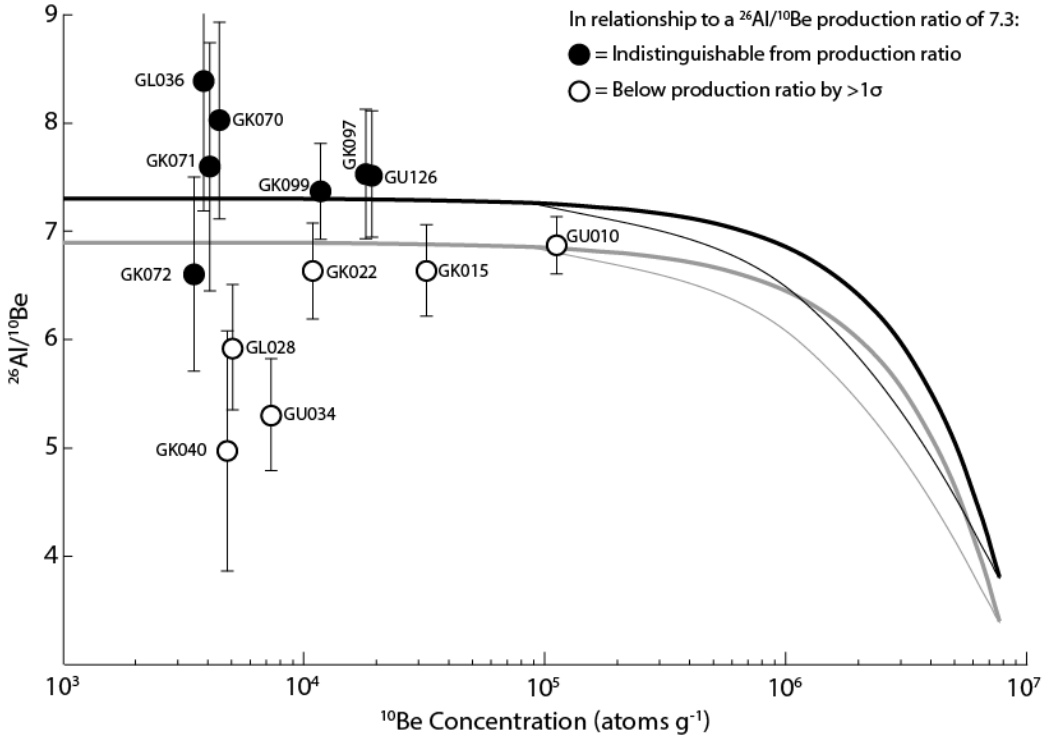

Figure 6.
(Width = 140 mm, 1.5 columns)

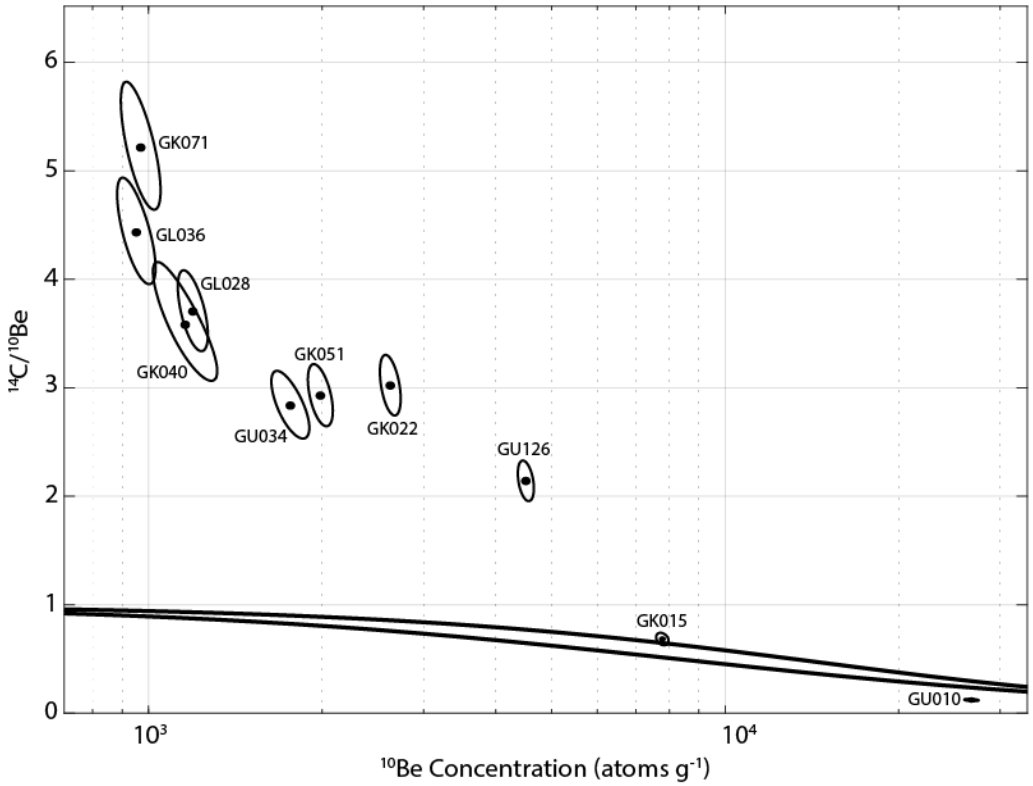

Figure 7.
(Width = 140 mm, 1.5 columns)

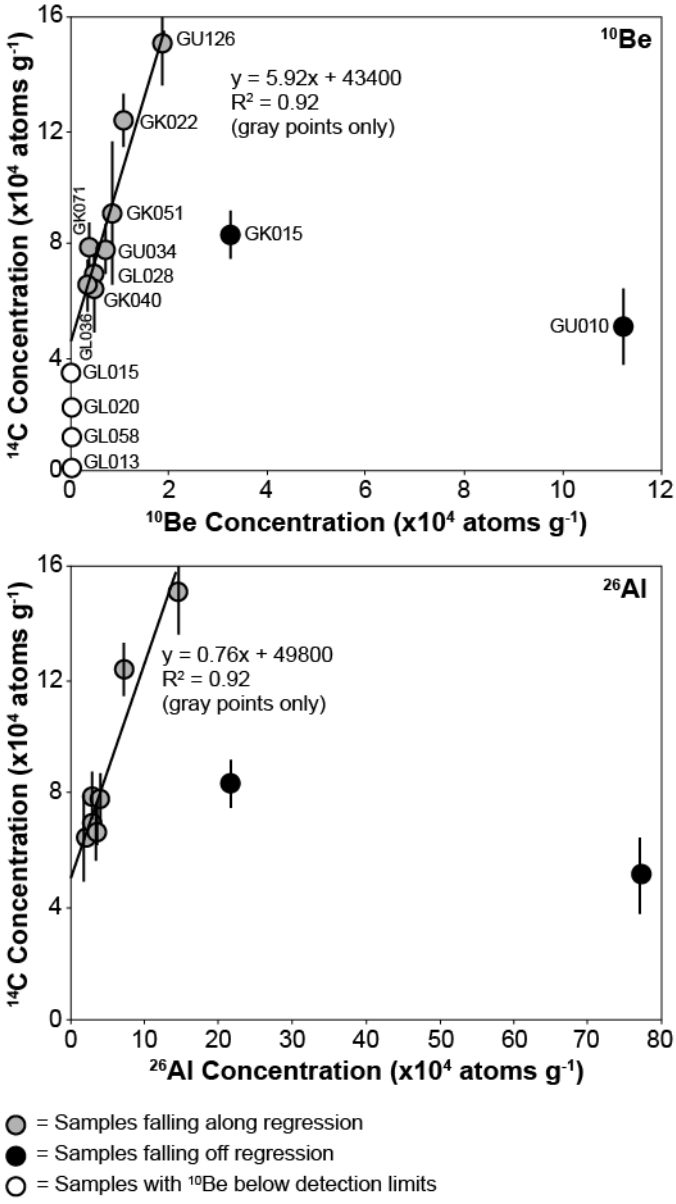

Figure 8.
(Width = 90mm, one column)

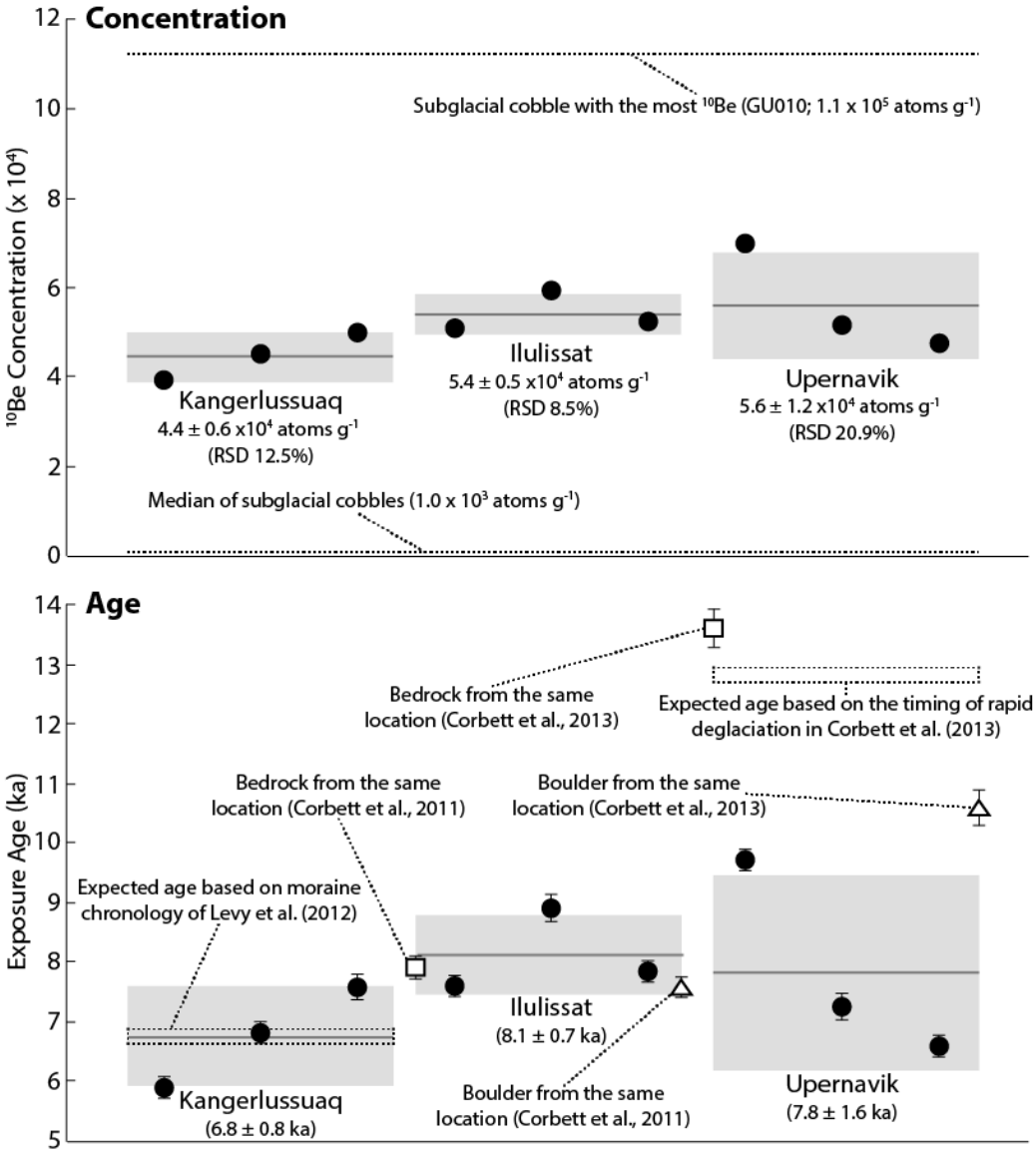

Figure 9.
(Width = 140 mm, 1.5 columns)